THE PEOPLE'S DEMOCRATIC REPUBLIC OF ALGERIA
الجمـــهوريـــة الجـــزائريـــة الديـمقـراطيـــــة الشـــعبيـــة
THE MINISTRY OF HIGHER EDUCATION AND SCIENTIFIC RESEARCH
وزارة التعـلـيـم الـعـالـــي والـبـحـث الـعـلـمي
AMAR TELIDJI UNIVERSITY OF LAGHOUAT
جـامـعـة عمّـــار ثـلـيـــجـــي بالأغـــواط
FACULTY OF TECHNOLOGY
كلية التكنولوجيا
DEPARTMENT OF ELECTROTECHNIC
قسم الالكتروتقني

Master's dissertation

Domain : Science and Technology
Field : Automatic
Option : Automatic and systems

By :

Kaf Fella Fatima Zohra ***Slimani Zoubida Nada***

THEME

Advanced Control of DC-DC Converters: Design & Simulation

Jury members:

Mr. RAYANE Khaled	***M.C. B***	***President***
Mr. OUBBATI Khalil Brahim	***M.C. B***	***Examinator***
Mr. BENMILOUD Mohamed	***M.C. B***	***Invited***
Mr. RAHMANI Belkacem	***M.C. B***	***Supervisor***
Mr. HADJAISSA Aboubakeur	***M.C. A***	***Co-supervisor***

Academic year 2024/2025

Acknowledgements

We would like to express our deep gratitude to our supervisor, Dr.Rahmani Belkacem, for his valuable guidance, continuous support, and great encouragement throughout the course of this research. His knowledge and extensive expertise were essential to the successful completion of this work.

We also extend our sincere appreciation to the members of the examination committee for their thorough review, critical insights, and constructive suggestions, which significantly contributed to improving the quality of this study. Their academic dedication and experience are truly commendable.

Our heartfelt thanks go to our families for their unwavering support, patience, and encouragement, which have been a constant source of strength and motivation throughout this journey.

Finally, we would like to thank the faculty and administrative staff of the Faculty of Technology for their dedication in providing a stimulating learning environment and the academic support that enabled us to complete this research successfully.

Thank you all for your guidance, direction, and valuable contributions. This work would not have been possible without your support and encouragement.

ملخص

يهدف هذا العمل إلى تصميم وتنفيذ استراتيجية تحكم فعالة لمحـول الدفع-السحب باستخدام تقنية التحكم النشط في الاضطرابات (ADRC). تم أولاً تطوير النموذج الرياضي المتوسط للمحول لتمثيل سلوكه الديناميكي بطريقة مناسبة للتحكم، ثم صُمم المراقب الموسع للحالة (ESO) لتقدير الحالات غير المقاسة والاضطرابات الخارجية. تم ضبط مكاسب المتحكم حسب عرض الحزمة المطلوب لضمان استجابة ديناميكية سريعة واستقرار قوي. تم تنفيذ محاكاة النظام بالكامل في بيئة (Simulink) باستخدام كتل (MATLAB Function) لتمثيل كل من النموذج وقانون التحكم. كما تم تنفيذ متحكم (PID) كلاسيكي معدل بغرض المقارنة. أُجريت المحاكاة تحت ثلاث سيناريوهات تشمل تغيّر الجهد المرجعي، جهد مصدر التغذية، وحمل المطبق. أظهرت النتائج تفوق المتحكم (ADRC) من حيث سرعة الاستجابة، تقليل تجاوز القيمة المرجعية، والقدرة على مقاومة الاضطرابات.

Résumé

Ce travail vise à concevoir et implémenter une stratégie de commande efficace pour un convertisseur push-pull en utilisant la technique du Contrôle Actif du Rejet de Perturbations (ADRC). Le modèle mathématique moyen du convertisseur a d'abord été développé afin de représenter dynamiquement le comportement du système. Un Observateur d'État Étendu (ESO) a été conçu pour estimer les états non mesurés et les perturbations. Les gains du contrôleur ont été ajustés selon la bande passante souhaitée pour assurer une réponse rapide et une stabilité robuste. Le Simulation complet de système a été implémenté dans Simulink en utilisant des blocs MATLAB Function pour la modélisation et le contrôle. Un PID classique modifié a aussi été réalisé à des fins de comparaison. Trois scénarios de simulation ont été testés, incluant des variations de la consigne, de la tension d'entrée et de la charge. Les résultats ont confirmé la supériorité de l'ADRC en termes de rapidité, de réduction du dépassement et de robustesse.

Abstract

This work aims to design and implement an efficient control strategy for a push-pull converter using the Active Disturbance Rejection Control (ADRC) technique. The averaged mathematical model of the converter was developed to accurately represent its dynamic behavior for control purposes. An Extended State Observer (ESO) was constructed to estimate unmeasured states and disturbances. The controller gains were tuned based on the desired bandwidth to ensure fast response and robust stability. The system Simulation was implemented in Simulink using MATLAB Function blocks for both modeling and control. A modified classical PID controller was also implemented for performance comparison. Simulations were conducted under three scenarios involving changes in reference voltage, input voltage, and load resistance. The results showed that ADRC offers superior performance in terms of speed, overshoot reduction, and disturbance rejection capability.

Table of Contents

List of Figures

Chapter 1

Introduction and Literature Review

1.1 General Introduction

In the midst of rapid technological advancement, the need for high-efficiency electrical energy conversion has become vital, especially in embedded systems, renewable energy applications, and industrial systems. DC-DC converters are among the most fundamental components in these systems due to their ability to reliably and efficiently adjust voltage and current levels. Among these topologies, the push-pull converter stands out for its simplicity, efficiency, and ability to handle medium to high power levels [12], [4]. Its symmetrical design allows it to provide good transformer utilization and effective energy transfer [2, 6, 12].

The Figure 1.1 below represents a simplified diagram of a solar power chain with the push-pull converter:

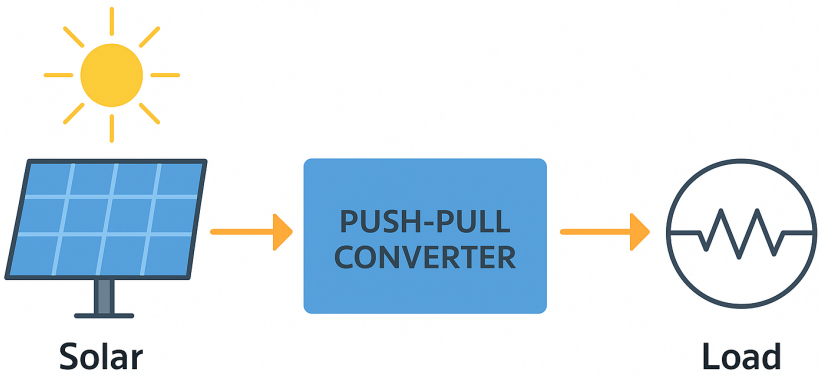

Figure 1.1: Photovoltaic system overview.

1.2 Literature Review

In recent years, increasing attention has been given to advanced control strategies in power electronics. Various algorithms such as adaptive control, fuzzy logic control, and model predictive control (MPC) have been explored to address system nonlinearity and disturbances. Among these, ADRC has emerged as a particularly promising solution. Some of these examples are introduced in [17, 13, 10, 11]. ADRC is based on the idea of rejecting disturbances actively using an Extended State Observer, thus reducing the dependence on precise system modeling.

Studies like [5, 14, 8, 9] have further demonstrated the effectiveness of ADRC and ESO in power electronic applications, highlighting their robustness and fast dynamic response. Despite these advances, the implementation of ADRC in push-pull converters remains relatively underexplored, presenting an opportunity for valuable contributions in this area. This research addresses this gap by applying and evaluating ADRC control in a push-pull converter system through detailed modeling and simulation analysis.

1.3 Problem Statement

Despite the advantages offered by the push-pull converter in terms of efficiency and galvanic isolation, controlling its output under varying operating conditions remains a complex task that poses significant challenges. These challenges become more pronounced in dynamic environments, where sudden load changes, input voltage fluctuations, and component tolerances introduce disturbances that give rise to system nonlinearities and uncertainties. Conventional control strategies, such as PID controller, are widely implemented due to their simplicity and ease of design [7, 15, 1, 3]. However, they often lack the robustness and adaptability when the system behavior deviates from its nominal conditions. These limitations underscore the need for more robust and adaptive control strategies [16].

1.4 Proposed Solution

To address these limitations, more robust and flexible control strategies are required. Therefore, researchers have increasingly turned to advanced control techniques that can offer improved disturbance rejection and adaptive performance. One such promising technique is Active Disturbance Rejection Control (ADRC), [5, 14, 8, 9] , owing to its model-free structure and the incorporation of an Extended State Observer (ESO) to estimate and compensate for disturbances in real time, enabling improved dynamic response and enhanced system stability.

1.5 Objectives of the Study

The objectives of this work is:

— Develop an accurate mathematical model for the push-pull DC-DC converter using state-space equations.
— Design an advanced ADRC-based control system to mitigate disturbances and enhance dynamic performance.
— Perform a comparative study between ADRC and conventional control methods through simulation.
— Analyze system stability and evaluate the effectiveness of the Extended State Observer (ESO).

1.6 Importance of the Study

The significance of this research lies in its potential contributions to the field of power electronics:

— Improving the dynamic stability of power converters under varying operational conditions.
— Reducing the sensitivity of the system to sudden changes or modeling uncertainties.
— Providing a practical and efficient control solution that can be extended to real world applications.

Chapter 2

Modeling and Analysis of the Push-Pull Converter

2.1 Introduction

Unlike simpler converters such as the buck or boost, the push-pull converter employs a center-tapped transformer and two active switches to enable bidirectional energy transfer during each switching cycle, allowing better transformer core utilization and reduced current ripple.

The following Figure 2.1 illustrates the classification of DC-DC converters:

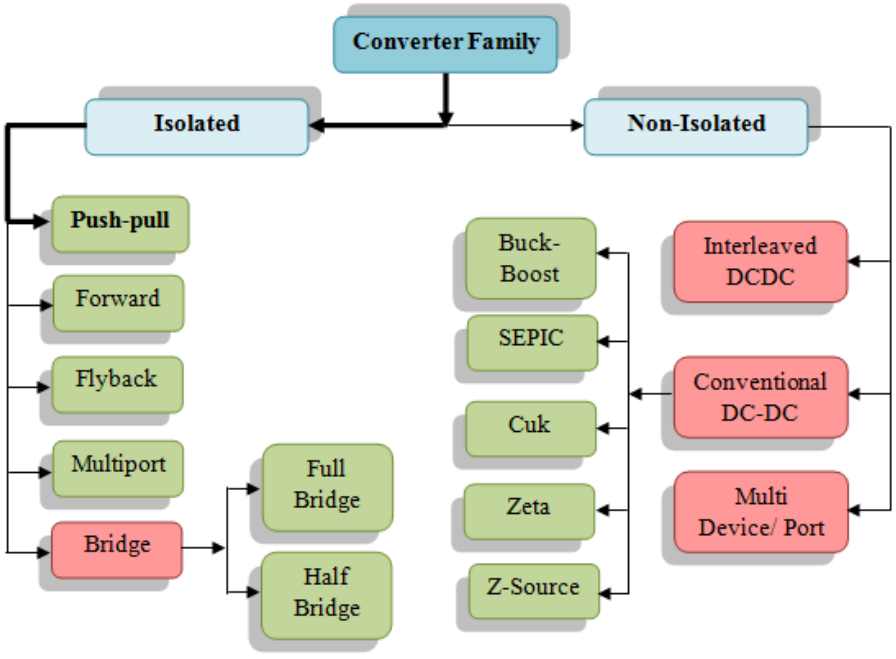

Figure 2.1: DC-DC Converter family.

Due to its transformer based architecture, the push-pull converter provides voltage step-up or step-down capabilities depending on the transformer turns ratio, making it ideal for applications like renewable energy systems, battery charging circuits, and isolated power supplies [6, 2].

To accurately predict and control the behavior of this converter, it is essential to develop a mathematical model that reflects its real dynamic characteristics. This chapter presents a detailed analysis of the push-pull converter's circuit operation, its average model derivation, and the simulation parameters that will be used in the control design phase.

2.2 Circuit Description

The push-pull converter typically consists of the following components [6, 2], as shown in Figure 2.2:

— A DC voltage source V_{in}, Output voltage V_o.
— Two electronic switches, usually MOSFET transistors Q_1, Q_2.
— Two diodes for rectification D_1, D_2.
— A filter capacitor C, filter inductor L and load resistor R.
— A transformer with a center-tapped primary winding and a secondary winding (turns ratio $n = N_2/N_1$).

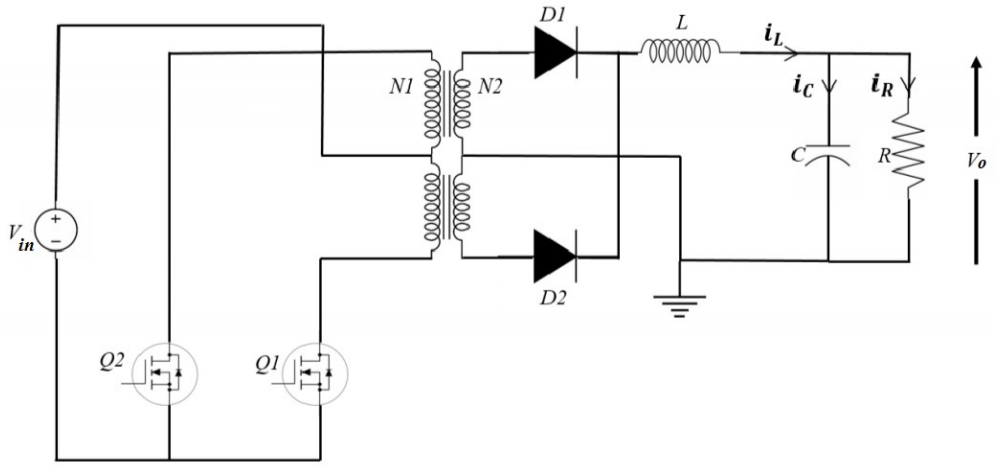

Figure 2.2: Circuit diagram of push-pull converter.

2.3 The Operational Principle of the Converter

The converter operates based on the alternating conduction of the switches:

— When the first switch is turned on, energy flows through the first half of the transformer's primary winding.
— When the second switch is turned on, energy flows through the second half.

This alternating switching ensures magnetic balance within the transformer core and maintains continuous conduction of current to the load.

In practical operation, the switches (denoted as Q_1 and Q_2) are controlled in a complementary manner. When Q_1 conducts, the magnetic field builds up in one direction within the transformer core, and when Q_2 conducts, it builds in the opposite direction. This symmetric operation improves core utilization and helps avoid magnetic saturation.

The alternating voltage generated on the secondary side is rectified by diodes (D_1 and D_2) and then filtered using a capacitor to provide a smooth DC output voltage. The transformer's turns ratio and the duty cycle of the switches together determine the relationship between the input and output voltages.

The Figure 2.3 shows the PWM duty cycle and its effect on Average output voltage:

The duty cycle:

$$u = \frac{T_{\text{on}}}{T}$$

Where:

— $\boldsymbol{T_on}$: Time
— $\boldsymbol{T}$: Duration Time

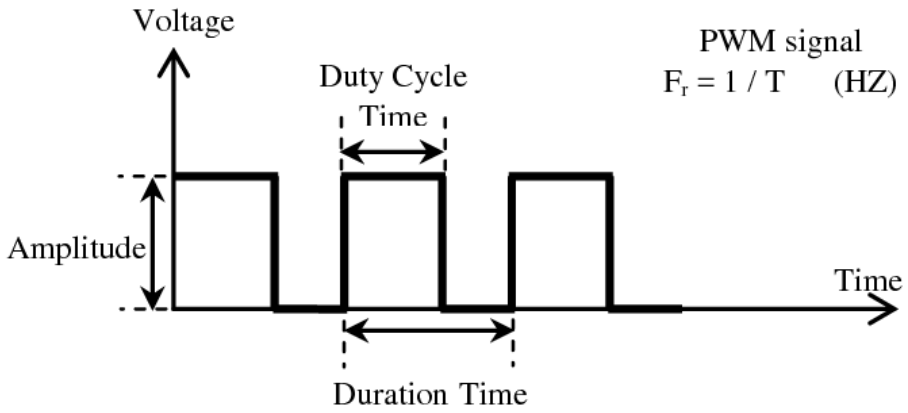

Figure 2.3: PWM duty cycle.

2.4 Modeling Assumptions

To simplify the mathematical model of the converter, the following assumptions are adopted:

— All components are ideal (i.e., no losses are considered).
— The switches operate in full alternation without any overlap.
— The converter operates at a high switching frequency, allowing the application of average modeling.
— The system operates in Continuous Conduction Mode (CCM).
— Equivalent Series Resistance (ESR) and transformer leakage inductance are neglected.
— The input voltage is assumed to be constant during each switching cycle.

2.5 Derivation of the Averaged Mathematical Model of the Push-Pull Converter

The mathematical model of the push-pull converter is derived by analyzing its two main modes of operation using the state-space representation approach. In this representation, the output voltage across the capacitor V_o and the inductor current i_L are selected as state variables ($x_1 = i_L$ and $x_2 = V_o$), while the final output voltage and current V, I are considered output variables.

The system is described by the following equations:

$$\dot{\boldsymbol{x}} = \boldsymbol{A}\boldsymbol{x} + \boldsymbol{B}\boldsymbol{u} \tag{2.1}$$

$$\boldsymbol{y} = \boldsymbol{C}\boldsymbol{x} + \boldsymbol{E}\boldsymbol{u} \tag{2.2}$$

Where:

— $\boldsymbol{A}$: State matrix
— $\boldsymbol{B}$: Input matrix
— $\boldsymbol{C}$: Output matrix
— $\boldsymbol{E}$: Direct transmission matrix (typically zero)
— $\mathbf{x} : \begin{bmatrix} i_L & V_o \end{bmatrix}^T$ State vector
— $\mathbf{y} : \begin{bmatrix} V & I \end{bmatrix}^T$ Output vector
— $\mathbf{u}$: Control input

The two distinct modes of operation in the converter for the purpose of modeling are:

2.5.1 Mode 1: Active Mode (Switch ON)

In this mode, one of the switches Q_1 or Q_2 is turned ON, allowing energy transfer from the primary to the secondary side. As a result, the current through the inductor increases and charges the output capacitor, increasing the output voltage V_o.

This mode is active during the interval dT_s, where d is the duty cycle.

By applying Kirchhoff's Voltage Law (KVL) to the circuit, we obtain the following equation:

The state-space and output equation for Mode 1 are:

$$\begin{bmatrix} \frac{di_L}{dt} \\ \frac{dV_0}{dt} \end{bmatrix} = \begin{bmatrix} 0 & -\frac{1}{L} \\ \frac{1}{C} & -\frac{1}{RC} \end{bmatrix} \begin{bmatrix} i_L \\ V_0 \end{bmatrix} + \begin{bmatrix} \frac{V_{in}}{L}\frac{N_2}{N_1} \\ 0 \end{bmatrix} [u] \tag{2.3}$$

$$y = \begin{bmatrix} 0 & 1 \end{bmatrix} \begin{bmatrix} i_L \\ V_0 \end{bmatrix} \tag{2.4}$$

2.5.2 Mode 2: Freewheeling Mode (Switch OFF)

In this mode, both switches Q_1 and Q_2 are OFF, and the stored energy in the inductor is released through the freewheeling diodes. No input voltage is applied during this period. This mode occurs over the remaining time interval $(1/2 - d)T_s$.

The state-space and output equation for Mode 2 are:

$$\begin{bmatrix} \frac{di_L}{dt} \\ \frac{dV_0}{dt} \end{bmatrix} = \begin{bmatrix} 0 & -\frac{1}{L} \\ \frac{1}{C} & -\frac{1}{RC} \end{bmatrix} \begin{bmatrix} i_L \\ V_0 \end{bmatrix} \tag{2.5}$$

$$y = \begin{bmatrix} 0 & 1 \end{bmatrix} \begin{bmatrix} i_L \\ V_0 \end{bmatrix} \tag{2.6}$$

2.5.3 Averaged Model of the Converter

To represent the converter's behavior over the entire switching period T_s, the time-averaging method is applied to combine both modes based on their time durations.

Given that:

$$\begin{aligned} A &= A_1 = A_2, \\ B &= 2dB_1, \\ C &= C_1 = C_2, \\ E &= 0 \end{aligned}$$

Thus, the final averaged model of the push-pull is:

$$A = \begin{bmatrix} 0 & -\frac{1}{L} \\ \frac{1}{C} & -\frac{1}{RC} \end{bmatrix}, \quad B = \begin{bmatrix} 2\frac{V_{in}}{L}\frac{N_2}{N_1} \\ 0 \end{bmatrix}, \quad C = \begin{bmatrix} 0 & 1 \end{bmatrix}, \quad E = \begin{bmatrix} 0 \end{bmatrix} \tag{2.7}$$

The representation in state-space:

$$\dot{x}_1 = -\frac{1}{L}x_2 + 2\frac{V_{in}}{L}\frac{N_2}{N_1}u \tag{2.8}$$

$$\dot{x}_2 = \frac{1}{C}x_1 - \frac{1}{RC}x_2 \tag{2.9}$$

$$y = x_2 \tag{2.10}$$

2.6 Conclusion

In this chapter, the average mathematical model of the push-pull converter was presented using state-space representation, based on the analysis of the two main operating modes and their integration into a unified model. This representation is a fundamental step toward accurately understanding the dynamic behavior of the converter and provides a solid foundation for designing future control systems.

This model enables the application of advanced control techniques such as Active Disturbance Rejection Control (ADRC).

Chapter 3

Design of The Active Disturbance Rejection Control (ADRC) System

3.1 Introduction

Active Disturbance Rejection Control (ADRC) has emerged as an innovative solution that does not rely on precise knowledge of the mathematical model. Instead, it actively estimates and compensates for disturbances in real time. This chapter aims to present the theoretical foundation of ADRC, demonstrate how the system model is reformulated to fit this approach, design the Extended State Observer (ESO), derive the control law, and provide an initial comparison with conventional control techniques.

3.2 Definition and Role of the Observer

The observer is a fundamental tool in control theory and signal processing. It allows the estimation of the internal states of a dynamic system based on its measured inputs and outputs. The Figure 3.1 presents the general block diagram of a state observer.

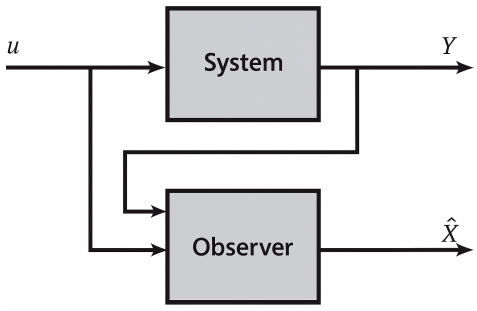

Figure 3.1: Block diagram of the observer.

3.3 Theoretical Origin of ESO: From Luenberger to ADRC

The Extended State Observer (ESO) used in ADRC shares conceptual foundations with the classical Luenberger observer. Both are designed to reconstruct the internal states of a system from measurable outputs. However, the ESO goes a step further by estimating not only the state variables but also the total disturbance, which includes model uncertainties and external perturbations.

Unlike the Luenberger observer, which requires an accurate system model and focuses solely on state estimation, the ESO embeds the unknown dynamics into an additional state variable. This approach enhances robustness and makes the control system less sensitive to modeling errors, thereby enabling real-time compensation of disturbances without explicit model knowledge. The Figure 3.2 presents the block diagram of the Luenberger observer.

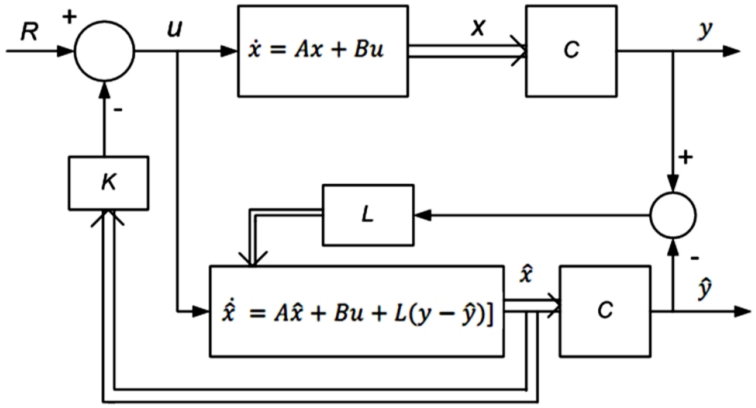

Figure 3.2: Block diagram of the Luenberger observer.

3.4 Principle of ADRC Operation

The ADRC relies on reformulating the structure of the dynamic system such that all unknown or unmodeled effects such as nonlinearities, time-varying parameters, and external disturbances are treated as a "total disturbance." An observer, known as the Extended State Observer (ESO), is designed to estimate both this total disturbance and the system state variables.

A key advantage of ADRC is its ability to function effectively without relying on an accurate mathematical model. This model-independence not only enhances robustness and adaptability in practical systems with complex or uncertain dynamics but also simplifies the design and implementation process.

The system consists of the following components:

— **Extended State Observer (ESO):** Estimates both the system state variables and the total disturbance in real time.
— **Control Law (PD controller):** Uses the estimated values from the ESO to generate the control input, which compensates for the disturbance effects and ensures accurate reference tracking.

The Figure 3.3 below represents the ADRC control structure.

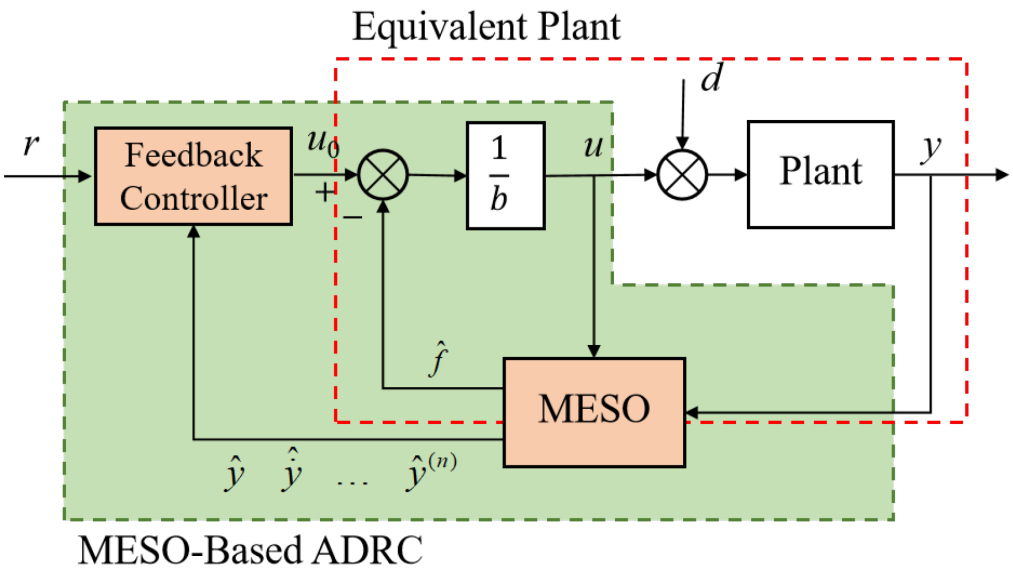

Figure 3.3: Block diagram of MESO-Based ADRC control structure.

Figure description

In this system, u represents the control input applied to the converter, which corresponds to the duty cycle ($0 < u < 0.5$). The output y is the measured voltage across the load. These two signals serve as the main inputs to the ADRC structure.

The Extended State Observer (ESO) estimates the system's state variables, which include the output voltage and its derivatives, along with the total disturbance. Based on these estimates, the control law generates the appropriate control signal u to compensate for disturbances and ensure accurate reference tracking.

3.5 Modified Mathematical Model for ADRC Implementation

To implement ADRC, the system's average model must be reformulated using flatness theroy to isolate the total disturbance, which includes all internal uncertainties, nonlinearities, and external disturbances into a total disturbance term $f(t)$, allowing simplified and robust control design. The system is typically expressed as a second-order differential equation:

$$\ddot{y} = f(t) + b_0 u \tag{3.1}$$

Where:

— $\boldsymbol{y}$: The system output.
— $\boldsymbol{u}$: The control input.
— $\boldsymbol{b_0}$: Nominal control gain.
— $\boldsymbol{f}$: The total disturbance.

3.5.1 Flatness-Based Control Simplification

Given that the push-pull converter is a second-order system and that its output variable (voltage) can be fully expressed in terms of its derivatives, the system can be classified as flat. Therefore, Flatness-Based Control (FBC) can be applied by directly expressing the input as a function of the output and its differential variables.

This modeling approach is particularly advantageous when designing advanced controllers such as ADRC, as it clarifies the relationship between input and output, and enables feed forward compensation of disturbances.

Flatness Transformation

Define the output as:

$$y = V_0 \tag{3.2}$$

Derive $\dot{y}$ and $\ddot{y}$ from the circuit equations:

$$\dot{y} = \dot{V_0} = \frac{1}{C} i_L - \frac{1}{RC} V_0 \tag{3.3}$$

$$\ddot{y} = \ddot{V_0} = \frac{1}{C} \frac{di_L}{dt} - \frac{1}{RC} \frac{dV_0}{dt} \tag{3.4}$$

$$\ddot{y} = \frac{1}{C} \left[-\frac{1}{L} V_0 + \frac{2V_{in}}{L} \frac{N_2}{N_1} u \right] - \frac{1}{RC} \left[\frac{dV_0}{dt} \right] \tag{3.5}$$

After expansion and simplification, we obtain:

$$\ddot{y} = -\frac{1}{RC}\dot{y} - \frac{1}{LC}y + \frac{2V_{in}}{LC}\frac{N_2}{N_1}u \tag{3.6}$$

Where:

$$b_0 = \frac{2V_{in}}{LC}\frac{N_2}{N_1} \tag{3.7}$$

$$f(t) = -\frac{1}{RC}\dot{y} - \frac{1}{LC}y \tag{3.8}$$

3.6 Design of the Extended State Observer (ESO)

To effectively estimate both the system states and the total disturbance, the Extended State observer (ESO) is employed. The key idea is to reformulate the original second-order system by augmenting it with an additional state that represents the total disturbance $f(t)$. The observer is then designed to estimate all three variables: the system output, its derivative, and the disturbance.

3.6.1 The state-space representation

We define the state variables as:

$$x_1 = y, \quad x_2 = \dot{y}, \quad x_3 = f(t) \tag{3.9}$$

The state-space representation becomes:

$$\dot{x}_1 = x_2 \tag{3.10}$$

$$\dot{x}_2 = x_3 + b_0 u = f(t) + b_0 u \tag{3.11}$$

$$\dot{x}_3 = \dot{f}(t) \tag{3.12}$$

This can be expressed in compact matrix where:

$$A = \begin{bmatrix} 0 & 1 & 0 \\ 0 & 0 & 1 \\ 0 & 0 & 0 \end{bmatrix}, \quad B = \begin{bmatrix} 0 \\ b_0 \\ 0 \end{bmatrix}, \quad E = \begin{bmatrix} 0 \\ 0 \\ 1 \end{bmatrix}, \quad C = \begin{bmatrix} 1 & 0 & 0 \end{bmatrix} \tag{3.13}$$

Consequently, the state space representation can be represented as follows:

$$\begin{pmatrix} \dot{x_1}(t) \\ \dot{x_2}(t) \\ \dot{x_3}(t) \end{pmatrix} = \begin{bmatrix} 0 & 1 & 0 \\ 0 & 0 & 1 \\ 0 & 0 & 0 \end{bmatrix} \cdot \begin{pmatrix} x_1(t) \\ x_2(t) \\ x_3(t) \end{pmatrix} + \begin{bmatrix} 0 \\ b_0 \\ 0 \end{bmatrix} \cdot u(t) + \begin{bmatrix} 0 \\ 0 \\ 1 \end{bmatrix} \cdot \dot{f}(t) \tag{3.14}$$

$$y(t) = \begin{bmatrix} 1 & 0 & 0 \end{bmatrix} \cdot \begin{pmatrix} x_1(t) \\ x_2(t) \\ x_3(t) \end{pmatrix} \tag{3.15}$$

In order to employ a control law, an extended state observer is needed to provide estimation.

3.6.2 The proposed observer

For disturbance estimation, the ESO is designed as:

$$\dot{\hat{x}} = A\hat{x} + Bu(t) + L(y - \hat{y}) \tag{3.16}$$

$$\hat{y} = C\hat{x} \tag{3.17}$$

Where:

— $\hat{x}$: $\begin{bmatrix} \hat{y}(t) & \hat{\dot{y}}(t) & \hat{f}(t) \end{bmatrix}^T$ The estimated state vector

— L: $\begin{bmatrix} L_1 & L_2 & L_3 \end{bmatrix}^T$ The observer gain vector

3.7 Calculation of the Observer Gain Vector L

To ensure the stability and fast response of the ESO, the observer gain L must be selected so that the poles of the matrix $A - LC$ are placed appropriately in the complex plane. This guarantees effective damping and fast estimation of both the system states and the total disturbance.

3.7.1 Method for calculating the observer gain

Based on the ESO equation (3.16), The poles of the matrix $A - LC$ are chosen to be faster than the closed-loop control poles. A common practical rule for placing the observer poles is:

$$S_{1,2,3}^{ESO} = (3 \text{ to } 10) \cdot S^{CL} \tag{3.18}$$

Where:

s^{ESO}: The selected pole locations for ESO.

S^{CL}: The desired closed-loop pole, typically estimated by:

$$S^{CL} \approx \frac{-6}{T_{settle}} \tag{3.19}$$

The s^{ESO} and s^{cL} formulations, along with thier corresponding pole values, were directly adopted from the ADRC literature [8].

3.7.2 Settling time (T_{settle})

It is the time required for the system output to remain within a certain percentage (typically 2% or 5%) of its final value after a sudden change in the reference signal. It is used as a benchmark to determine the speed of the system's response and control performance.

First, the 2% settling time T_{settle} is selected as a performance criterion, then the closed loop S^{CL} and s^{ESO} are calculated to achieve a rapid response and system stability.

Using this estimation, the characteristic polynomial of $A - LC$ is defined as:

$$\begin{aligned} \det(sI - (A - LC)) &= s^3 + l_1 s^2 + l_2 s + l_3 \\ &= (s - s^{ESO})^3 \\ &= s^3 - 3s^{ESO} \cdot s^2 + 3 \cdot (s^{ESO})^2 \cdot s - (s^{ESO})^3 \end{aligned} \tag{3.20}$$

Once the pole locations are chosen, the gain coefficients are computed as:

$$l_1 = -3 \cdot s^{ESO} \tag{3.21}$$

$$l_2 = 3 \cdot (s^{ESO})^2 \tag{3.22}$$

$$l_3 = -(s^{ESO})^3 \tag{3.23}$$

Thus, the observer gain vector L is defined as:

$$L = \begin{bmatrix} l_1 \\ l_2 \\ l_3 \end{bmatrix} \tag{3.24}$$

3.8 Control Law

The control law in the ADRC strategy relies on the outputs of the ESO, which estimates both the system states and the total disturbance in real time. The objective of the control law is to generate a control signal $u(t)$ that compensates for disturbances and ensures accurate tracking of the reference signal y_{ref}.

3.8.1 The proposed controller

To obtain the actual control signal, the estimated total disturbance $\hat{f}(t)$ is compensated as follows:

We propose controller:

$$u(t) = \frac{1}{b_0}\left(u_0 - \hat{f}(t)\right) \tag{3.25}$$

By substituting $u(t)$ in the ESO equation (3.1), we obtain:

$$\dot{y} = f(t) + b_0\left(\frac{1}{b_0}\left(u_0 - \hat{f}(t)\right)\right) = u_0 + \left(f(t) - \hat{f}(t)\right) \approx u_0 \tag{3.26}$$

A modified **Proportional-Derivative (PD)** controller is employed, expressed as:

$$u_0(t) = \ddot{y}_{ref} - k_p e - k_d \dot{e} \tag{3.27}$$

Where:

— $\boldsymbol{e = y - y_{ref}}$
— $\boldsymbol{\dot{e} = \dot{y} - \dot{y}_{ref}}$
— $\boldsymbol{\hat{x}_1(t) = \hat{y}(t) \approx y(t)}$:is the estimated output.
— $\boldsymbol{\hat{x}_2(t) = \hat{\dot{y}}(t) \approx \dot{y}(t)}$:is the estimated of the first derivative of the output.
— $\boldsymbol{\hat{x}_3(t) = \hat{f}(t) \approx f(t)}$:is the estimated total disturbance.
— $\boldsymbol{e}$:Tracking error.
— $\boldsymbol{y_{ref}}$:Reference signal.

Given that:

$$y_{ref} = \text{constant}, \quad \text{which means that:} \quad \dot{y}_{ref} = \ddot{y}_{ref} = 0 \tag{3.28}$$

A PD controller without the derivative part for the reference value y_{ref} will lead to closed loop behavior with adjustable dynamics:

$$u_0(t) = k_p\left(y_{ref} - y(t)\right) - k_d \cdot \dot{y}(t) \tag{3.29}$$

Thus, the final control input becomes:

$$u(t) = \frac{1}{b_0}\left(k_p\left(y_{ref} - \hat{x}_1(t)\right) - k_d \cdot \hat{x}_2(t) - \hat{x}_3(t)\right) \tag{3.30}$$

This control structure enables the system to achieve fast dynamic response while actively rejecting disturbances and modeling uncertainties, without requiring an accurate model of the plant.

3.8.2 Tuning of Control Gains K_p and K_d

The tuning of the proportional K_p and derivative K_d gains is based on the desired reference tracking performances, with the settling time T_{settle} commonly used as an indicator of system responsiveness.

The closed-loop poles were placed to achieve the desired dynamic performance, the corresponding control gains were calculated using the pole placement methodology:

The controller gains are expressed as:

$$K_p = (S^{CL})^2 \tag{3.31}$$

$$K_d = -2S^{CL} \tag{3.32}$$

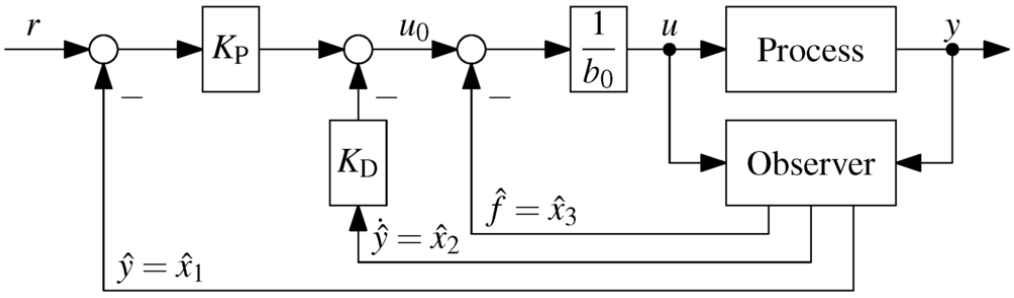

Figure 3.4: Control loop structure with ADRC for second-order process.

Figure Description

The figure illustrates the control loop structure of a second-order ADRC. When disturbances or model uncertainties affect the system, the Extended State Observer (ESO) estimates them in real time. The tracking error is computed as the difference between the reference signal and the

estimated output $\hat{y}(t)$. This error is processed by the PD controller to generate a virtual control signal $u_0(t)$. The estimated total disturbance $\hat{f}(t)$=$\hat{x_3}(t)$is then subtracted from . Finally, the actual control input $u(t)$ is applied to the system to ensure accurate tracking of the reference.

3.9 Comparative PID Controller Design

To evaluate the effectiveness of the ADRC approach, a conventional Proportional-Integral-Derivative (PID) controller was implemented in MATLAB-SIMULINK for performance comparison. Unlike a basic PID structure, the controller used here was carefully tuned based on the dynamic model of the push-pull converter. The PID gains were adjusted to achieve a comparable dynamic response, making the comparison with ADRC fair under identical operating conditions.

The Figure 3.5 below shows the standard block diagram of a conventional PID controller.

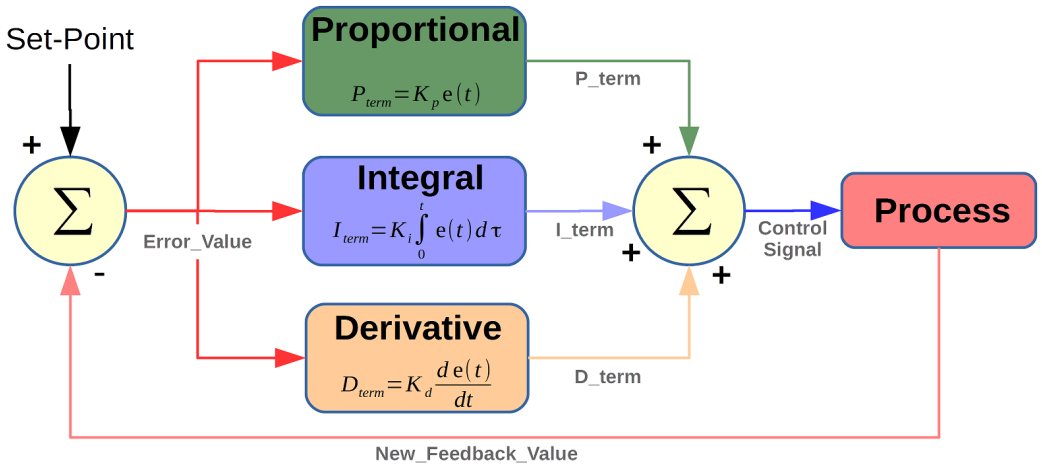

Figure 3.5: PID controller block diagram.

3.9.1 The state-space representation:

We define the state variables as:

$$x_1 = y, \quad x_2 = \dot{y}, \quad x_3 = \int_0^t y - y_{ref}\, d\tau \tag{3.33}$$

The state-space representation becomes:

$$\dot{x}_1 = x_2 \tag{3.34}$$

$$\dot{x}_2 = -\frac{1}{RC}x_2 - \frac{1}{LC}x_1 + b_0 u \tag{3.35}$$

$$\dot{x}_3 = x_1 - y_{ref} \tag{3.36}$$

This can be expressed in compact matrix where:

$$A_p = \begin{bmatrix} 0 & 1 & 0 \\ -\frac{1}{LC} & -\frac{1}{RC} & 0 \\ 1 & 0 & 0 \end{bmatrix}, \quad B_p = \begin{bmatrix} 0 \\ b_0 \\ 0 \end{bmatrix}, \quad E_p = \begin{bmatrix} 0 \\ 0 \\ 1 \end{bmatrix}, \quad C_p = \begin{bmatrix} 1 & 0 & 0 \end{bmatrix} \tag{3.37}$$

3.9.2 PID Control Law

The PID is designed as:

$$\dot{x} = A_p \cdot x + B_p \cdot u + E_p \cdot y_{ref} \tag{3.38}$$

$$y = C_p x \tag{3.39}$$

The PID controller used in this work is implemented in a state-space form rather than the classical time-domain formulation. The control input u is calculated as a linear combination of the system states:

$$u = -K \cdot x = -k_1 x_1 - k_2 x_2 - k_3 x_3$$

Where:

— $\boldsymbol{x_1}$: the output voltage (y), representing the proportional part of the controller.
— $\boldsymbol{x_2}$: the derivative of the output ($\dot{y}$), representing the derivative part.
— $\boldsymbol{x_3}$: the integral of the tracking error $\left(\int (y - y_{\text{ref}})\, dt\right)$, representing the integral part.
— $\boldsymbol{K = [k_1, k_2, k_3]}$: the gain vector selected using the pole placement method to ensure system stability and desired performance.
— $\boldsymbol{u}$: the control signal applied to the converter switches.

This formulation provides a full PID behavior within a state-space framework, aligning with the system dynamics and enabling fair comparison with the ADRC-based approach.

Controller Gain Design via Pole Placement

To compute the gain vector $\mathbf{K} = [k_1, k_2, k_3]$, the pole placement method was applied to the state-space model :

$$\dot{x} = A_P x + B_p u$$

with the control law :

$$u = -Kx$$

The closed-loop poles of the matrix $(A_p - B_p K)$ were assigned to match the desired characteristic polynomial:

$$\lambda(A_p - B_p K) = (s + S^{CL})^3$$

This ensures a critically damped response with appropriate settling time. The coefficients k_1, k_2, and k_3 were then determined by matching this desired polynomial with the characteristic equation of the closed-loop system.

3.10 Conclusion

This chapter presented the design methodology of the ADRC controller, including the reformulation of the system model, the development of the Extended State Observer (ESO), and the derivation of the control law using pole placement. The tuning process was guided by desired performance metrics such as settling time. Additionally, a model-based PID controller was implemented to serve as a benchmark for performance comparison. This structured approach provides a solid foundation for evaluating the robustness and tracking accuracy of ADRC.

Chapter 4

Simulation and Results

4.1 Introduction

This chapter provides a comparative analysis of simulation results for a push-pull converter system controlled by the Active Disturbance Rejection Control (ADRC) method and a conventional PID controller. The simulations, conducted using MATLAB/Simulink, focus on assessing each controller's effectiveness in terms of tracking precision, dynamic response, and robustness against disturbances under different test scenarios.

4.2 System Setup

Table 4.1 shows the physical parameter of the push-pull converter used in the simulation:

Table 4.1: Electrical Circuit Component Values.

Component	Symbol	Value
Input voltage	V_{in}	100V
Transformer Turns Ratio	n	0.55
Inductor	L	700e-6 H
Capacitor	C	1.36e-3 F
Load resistance	R	10Ω

4.3 Tuning of Control and Observer Parameters

The algorithm design was based on the physical parameters of the converter, with a focus on systematically tuning both the Extended State Observer (ESO) and the controller to ensure a fast and stable dynamic response.

A desired settling time was selected $T_{settle} = 0.01s$, from which the closed-loop bandwidth $S^{CL} = -600$ was determined to achieve appropriate response speed. To accelerate the observer's response relative to the converter, this bandwidth was increased by a factor of 50 to obtain the observer bandwidth $s^{ESO} = -3000$

Based on this value, the third-order observer gains:

$$\mathbf{L} = [L_1, L_2, L_3]^T = [900000 \quad 2.700010^{11} \quad 2.700010^{16}]$$

were computed using s^{E50} to ensure accurate tracking of states and disturbances.

Finally, the control gains $K_p = 360000$ and $K_d = 1200$ were calculated, ensuring high precision performance and robust stability under varying load or input voltage conditions.

Figure 4.1 shows the diagram block of the ADRC and the system in the SIMULINK.

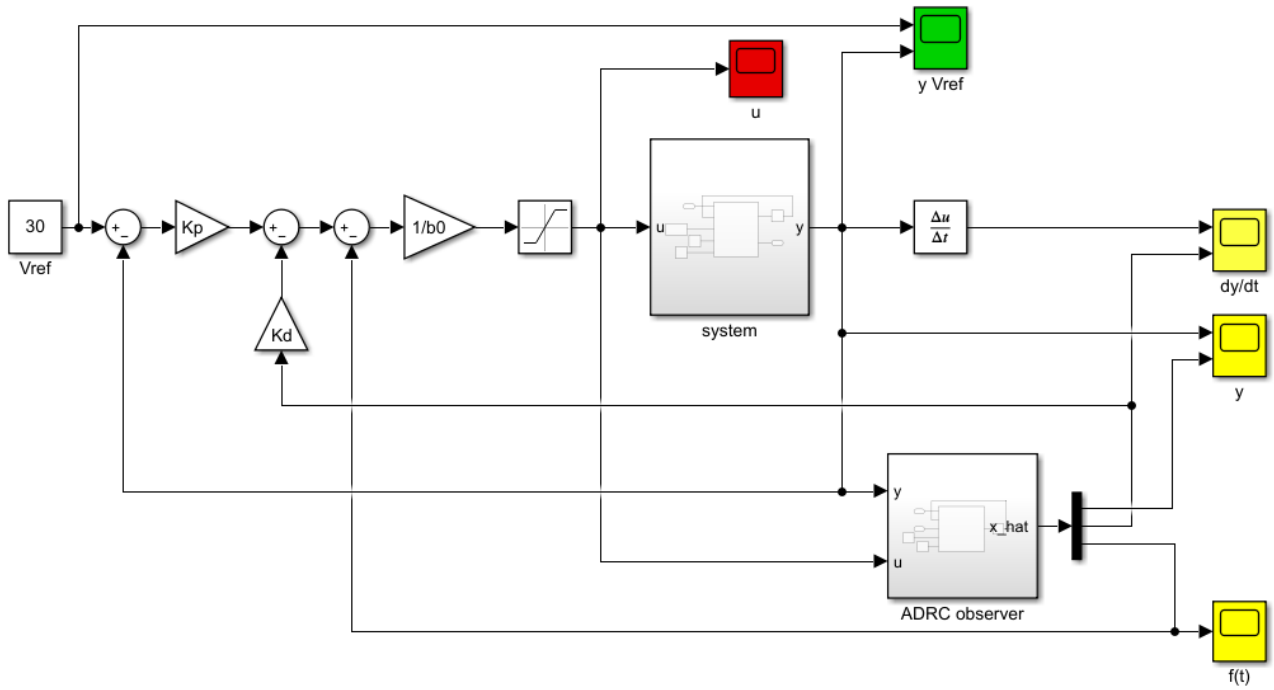

Figure 4.1: ADRC Structure with te system in MATLAB/Simulink.

4.4 Control Signal Generation

The control signal, representing the duty cycle, was directly generated from the output of each controller. To ensure safe converter operation, the duty cycle range was practically limited to [0.01, 0.48]. This constraint prevents the converter from entering unstable regions or stressing its components.

— **Theoretically:** $0 < u < 0.5$
— **Practically:** $0.01 < u < 0.48$

Note:

The reference voltage was selected within the safe operation range ($V_{ref} = 30V$). Given that the input voltage is 100V and the transformer turns ratio is 0.55, the theoretical output voltage ranges from 0 to 55V.

The state-space matrices were defined in the MATLAB Function blocks. Figure 4.2 represents the blocks used for modeling the converter and the ADRC.

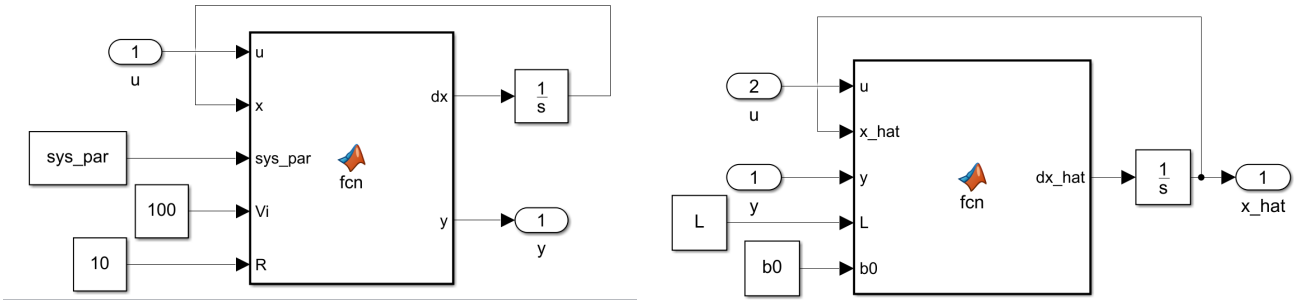

Figure 4.2: MATLAB Function Blocks for the Converter Model and ADRC.

The input vector sys_par was used to pass the three main parameters of the converter (L), (C), and (n) to the MATLAB Function block representing the converter model. This approach aims to simplify the model structure and reduce the number of inputs, making it easier to tune and update parameters when needed.

4.5 PID Controller Simulation

As a reference benchmark for comparison with ADRC controller, a modified PID controller was designed based on three main paths:

1. In the proportional path, the regulated output voltage was directly multiplied by the gain K_1.
2. In the derivative path, the voltage derivative was extracted from the ADRC output and then multiplied by the K_2.
3. In the integral path, the error between the output voltage and the reference signal was calculated and multiplied by the gain K_3, then passed through numerical integration.

The outputs of the paths were summed to obtain the control signal, which was constrained to ensure it remained within safe operating limits before being applied to the system.

Figure 4.3 shows the PID block diagram in SIMULINK.

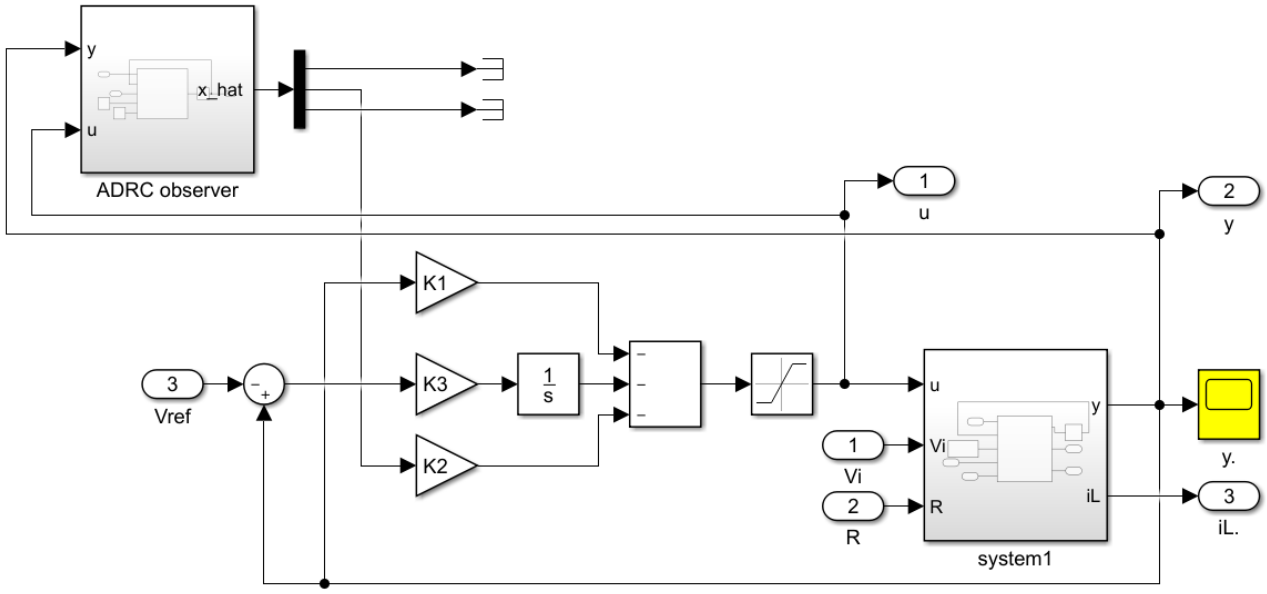

Figure 4.3: PID Controller in MATLAB/Simulink.

To achieve an appropriate dynamic response, the PID gains were tuned using the pole placement. The matrices A and B were defined, the gain vector K was calculated using the command:

$$K = \text{acker}(A_p, B_p, P_d) \tag{4.1}$$

Where: $P_d = [S^{CL}\ S^{CL}\ S^{CL}]$ is the desired poles.

4.6 Simulation Methodology and Performance Tests

The simulation was carried out under three main scenarios representing variations in reference voltage, input voltage, and load resistance, in order to test system stability and the effectiveness of each control strategy. These scenarios enable the evaluation of the system's response in dynamic environments.

Figure 4.3 shows the ADRC and PID controllers in SIMULINK under the operation conditions.

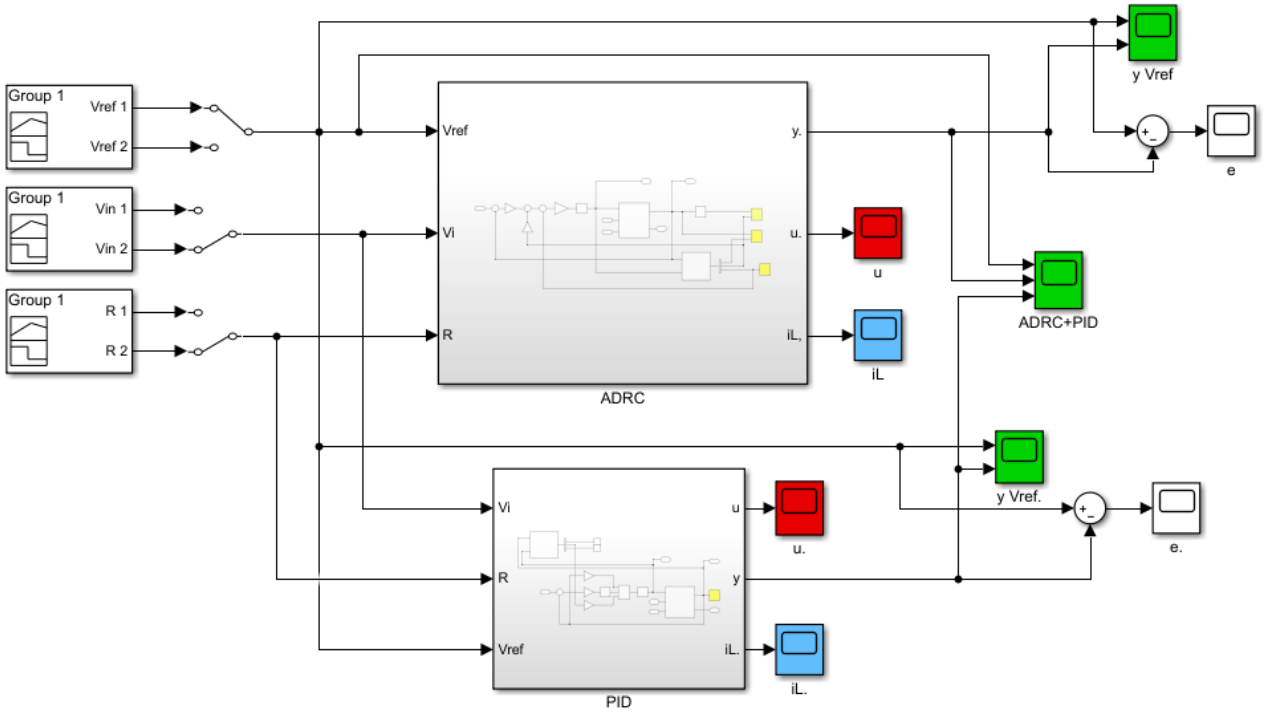

Figure 4.4: Comparison of ADRC and PID Controllers under Different Operating Conditions.

4.7 Simulation Scenarios

To analyze the dynamic response of the converter under PID and ADRC control, three main test scenarios were conducted:

4.7.1 Scenario 1:

In this scenario, the reference voltage V_{ref} is varied five times within one second, while both the input voltage V_{in}=100V, and load resistance R =10Ω are kept constant.

$$V_{\text{ref}}(t) = \begin{cases} 20\,\text{V} & \text{if } 0 \leq t < 0.2 \\ 25\,\text{V} & \text{if } 0.2 \leq t < 0.4 \\ 30\,\text{V} & \text{if } 0.4 \leq t < 0.7 \\ 22\,\text{V} & \text{if } 0.7 \leq t < 0.8 \\ 25\,\text{V} & \text{if } 0.8 \leq t < 1 \end{cases}$$

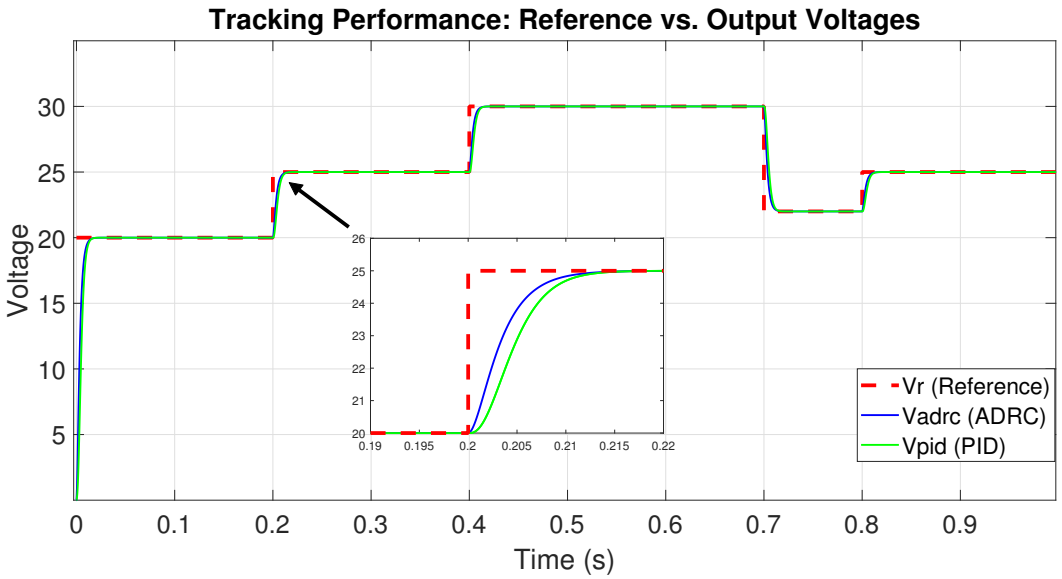

Figure 4.5: Comparison of Output Voltage (ADRC and PID) with the reference.

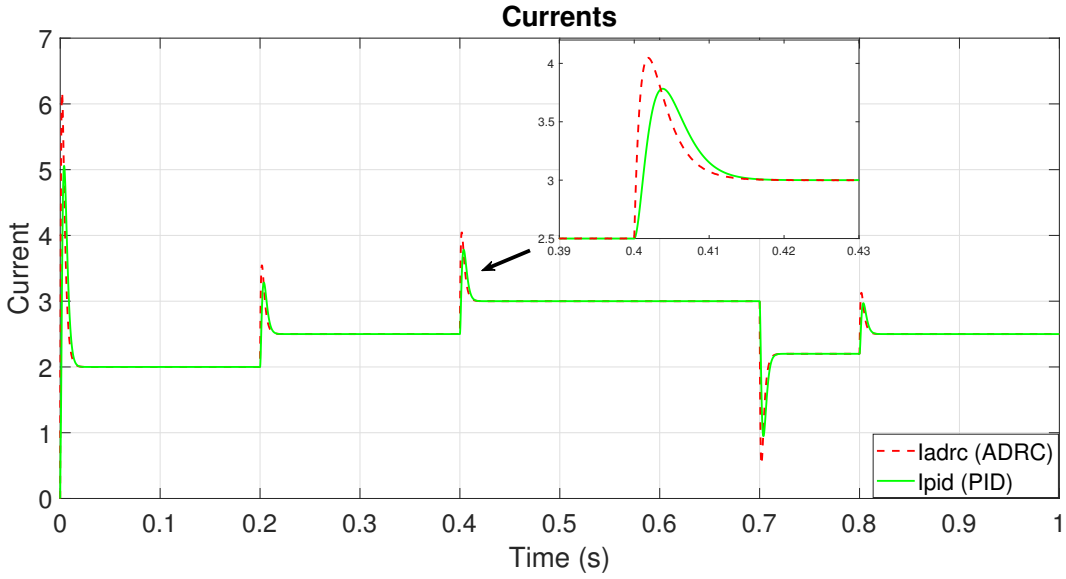

Figure 4.6: Inductor Current Comparison

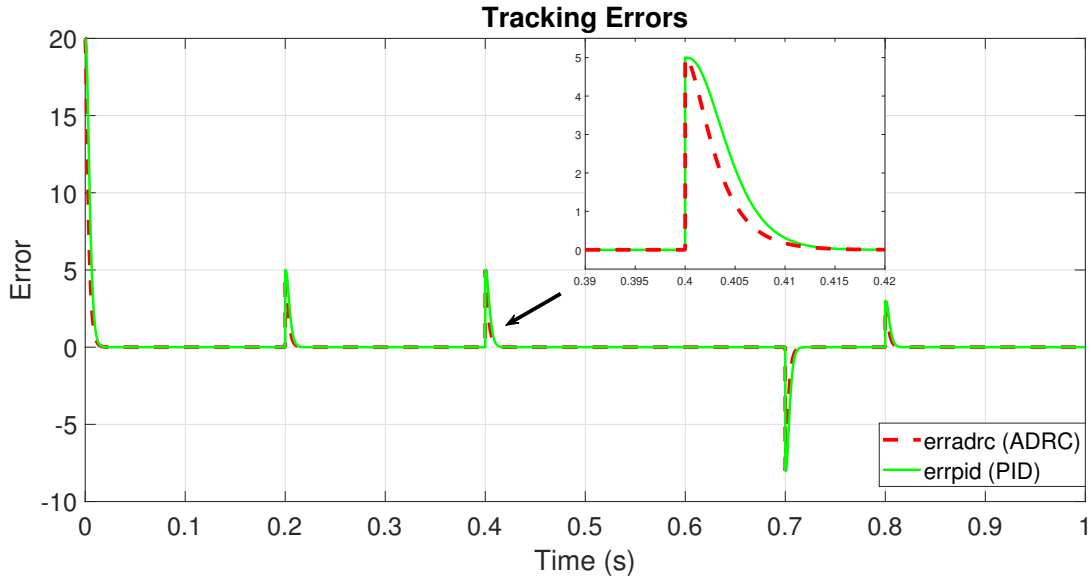

Figure 4.7: Tracking Error Comparison.

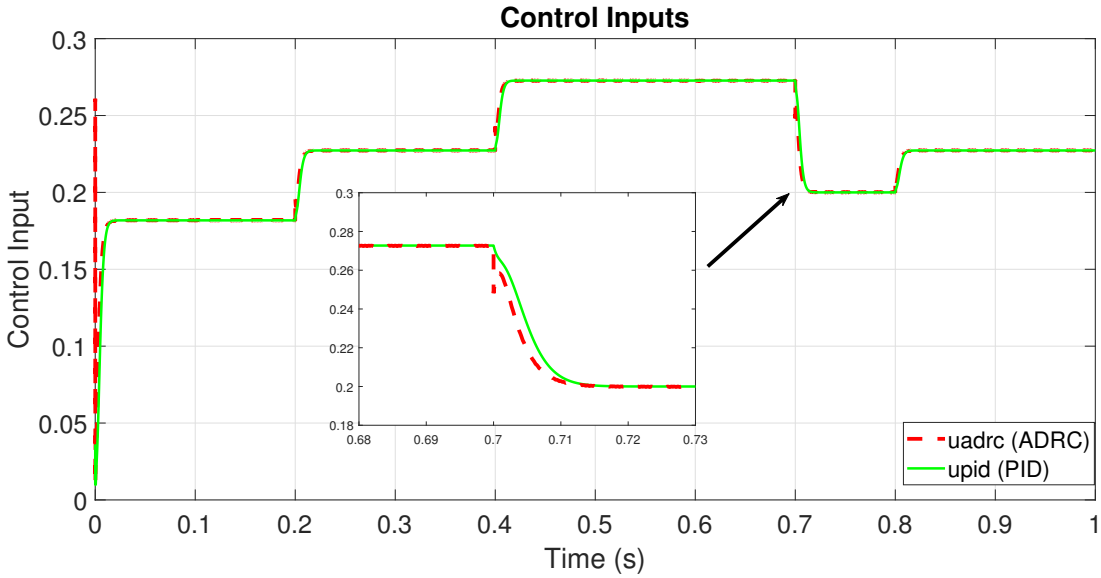

Figure 4.8: Control Signal Comparison

4.7.2 Scenario 2:

In this scenario, the reference voltage V_{ref}=30V, and load resistance R =10Ω are held constant, while the input voltage V_{in} is changed five times within one second. are kept constant.

$$Vin(t) = \begin{cases} 90\,\text{V} & \text{if } 0 \leq t < 0.1 \\ 100\,\text{V} & \text{if } 0.1 \leq t < 0.2 \\ 80\,\text{V} & \text{if } 0.2 \leq t < 0.5 \\ 95\,\text{V} & \text{if } 0.5 \leq t < 0.8 \\ 110\,\text{V} & \text{if } 0.8 \leq t < 1 \end{cases}$$

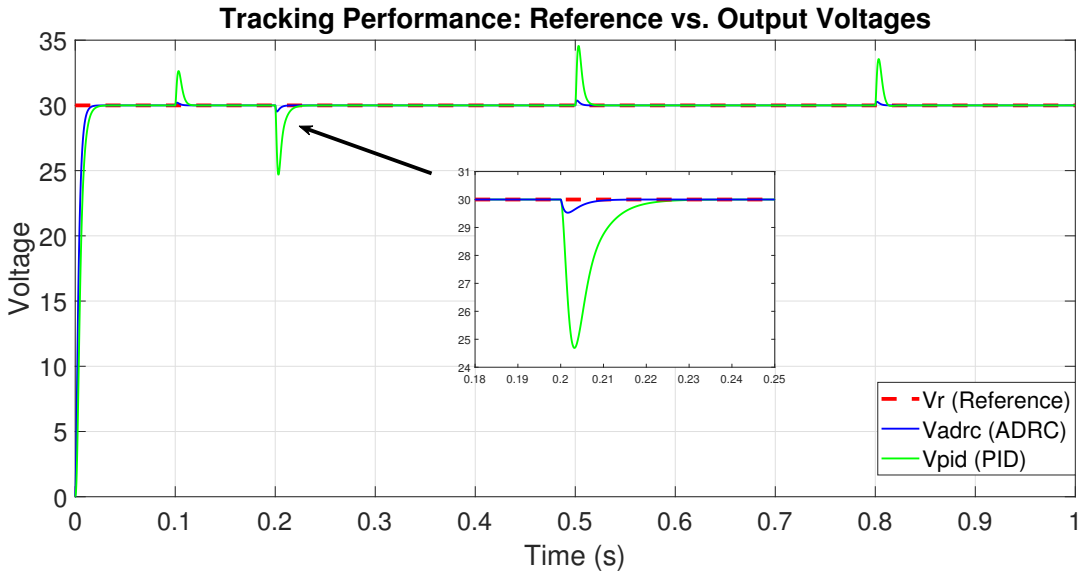

Figure 4.9: Comparison of Output Voltage (ADRC and PID) with the reference.

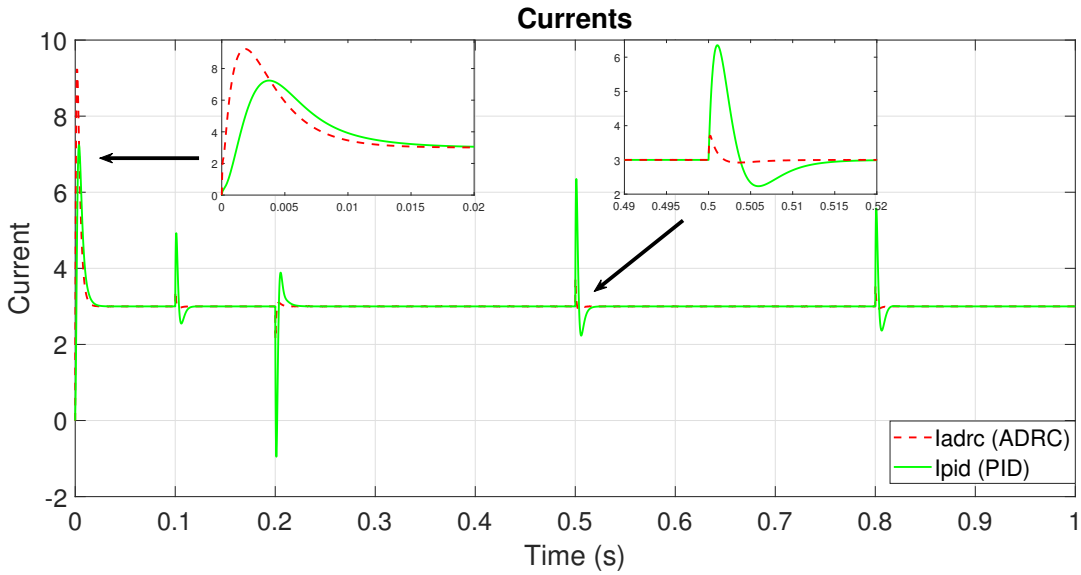

Figure 4.10: Inductor Current Comparison

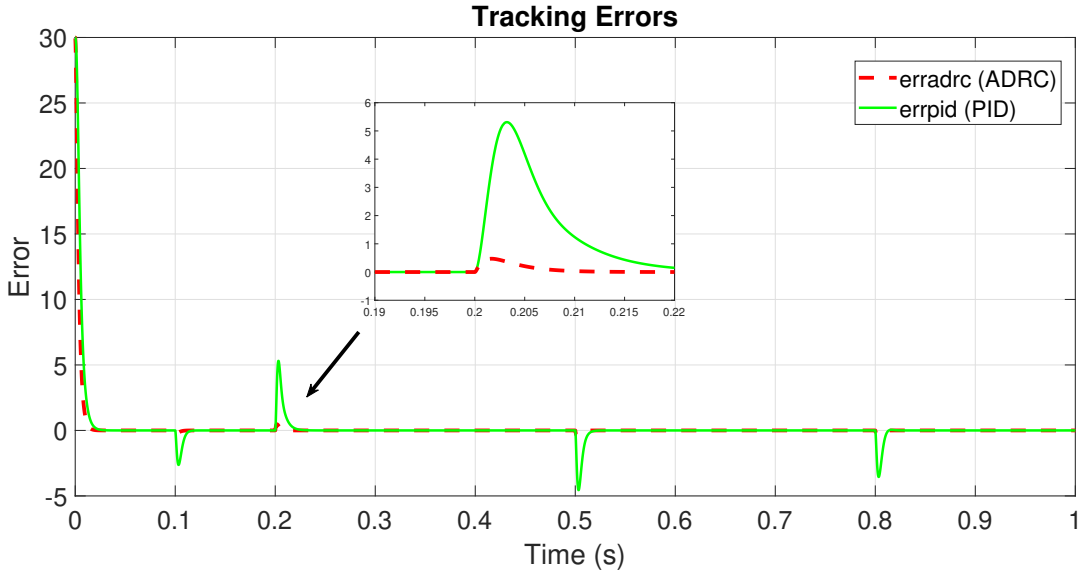

Figure 4.11: Tracking Error Comparison.

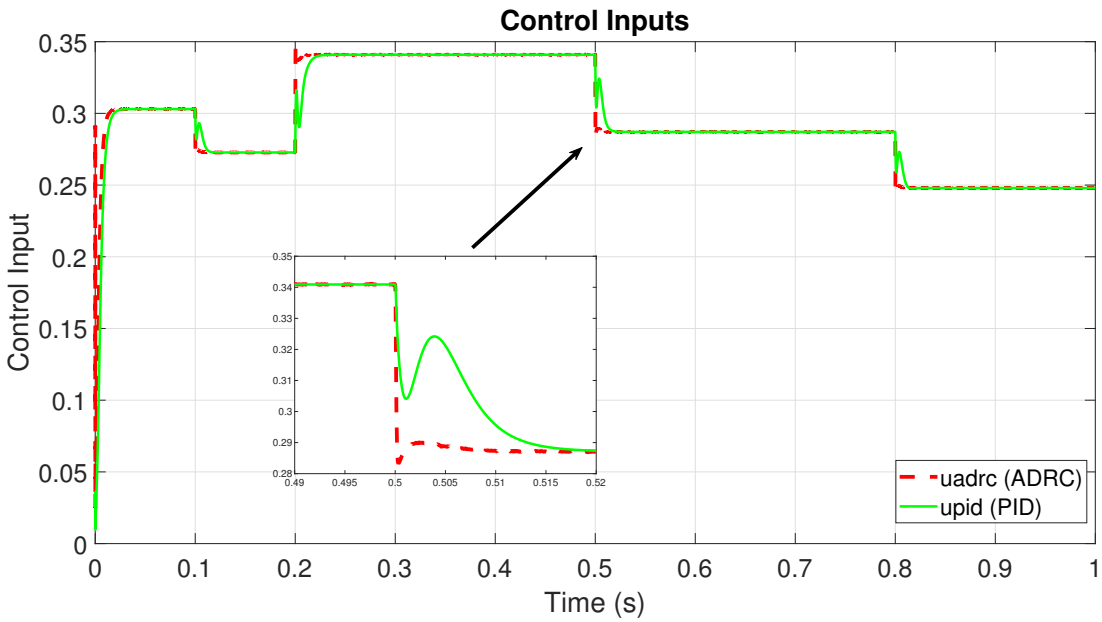

Figure 4.12: Control Signal Comparison

4.7.3 Senario 3:

In this scenario, the reference voltage V_{ref}=30V, and the input voltage V_{in}=100V are constant, while the load resistance R is changed five times within one second.

$$R(t) = \begin{cases} 10\,\Omega & \text{if } 0 \leq t < 0.3 \\ 5\,\Omega & \text{if } 0.3 \leq t < 0.4 \\ 12\,\Omega & \text{if } 0.4 \leq t < 0.5 \\ 15\,\Omega & \text{if } 0.5 \leq t < 0.6 \\ 9\,\Omega & \text{if } 0.6 \leq t < 1 \end{cases}$$

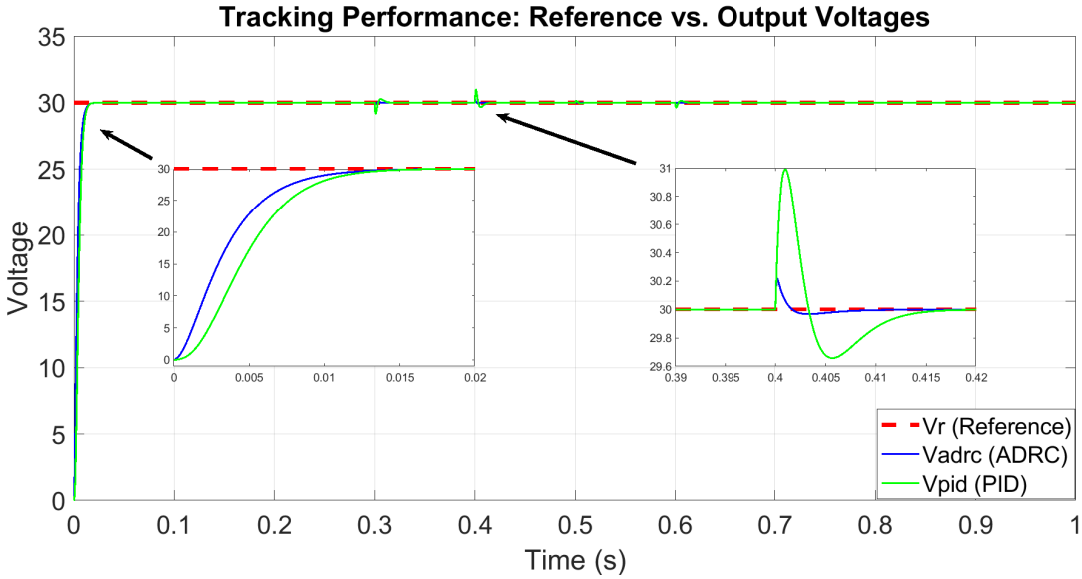

Figure 4.13: Comparison of Output Voltage (ADRC and PID) with the reference.

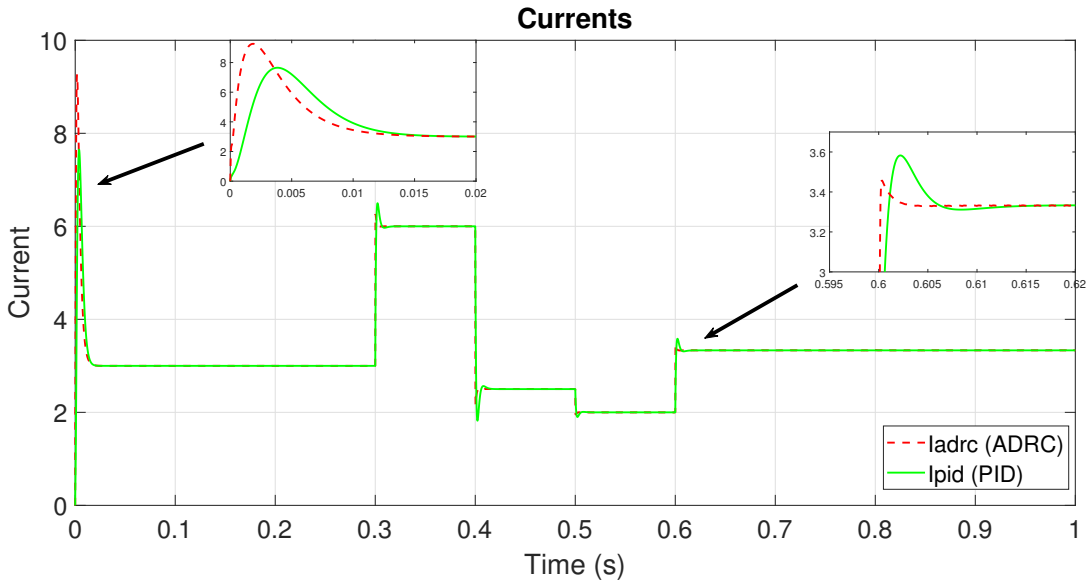

Figure 4.14: Inductor Current Comparison

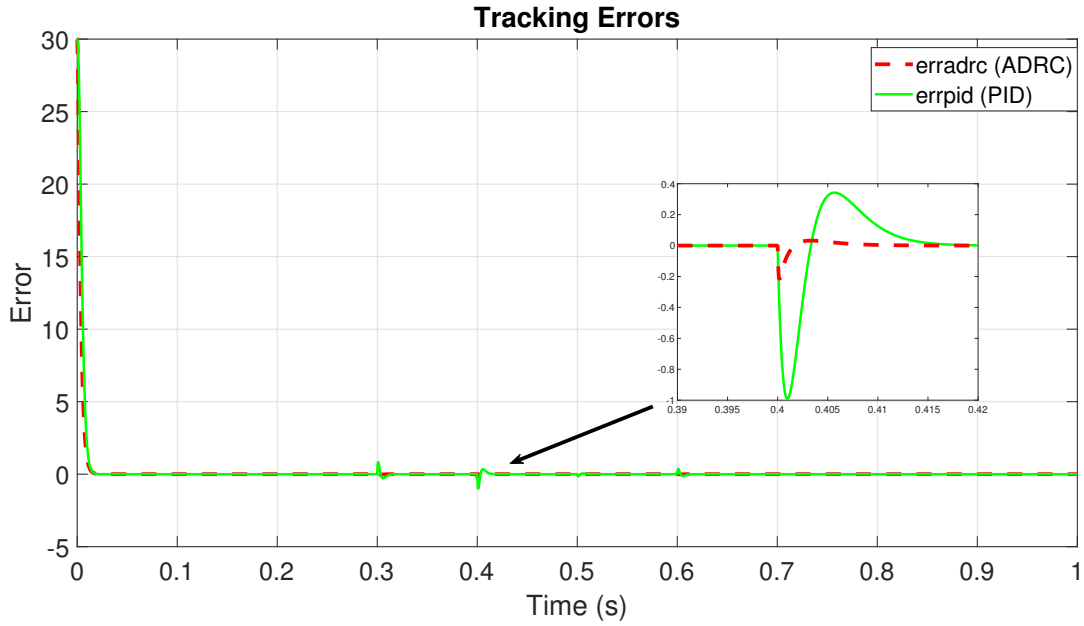

Figure 4.15: Tracking Error Comparison.

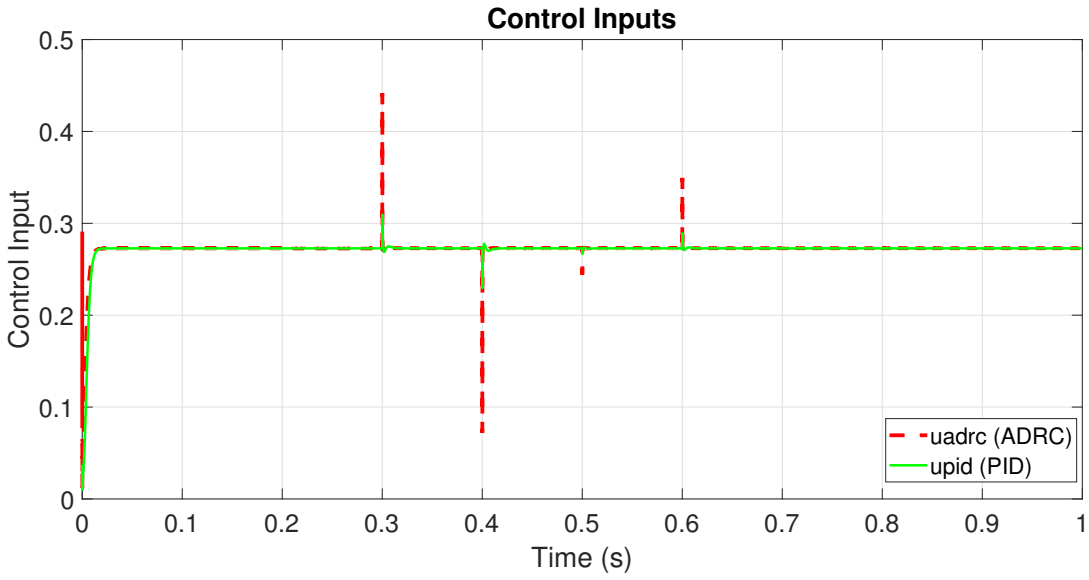

Figure 4.16: Control Signal Comparison

4.8 Results Analysis

The simulation results across the three scenarios clearly demonstrate the superior performance of the ADRC controller compared to the PID controller, even when the PID was finely tuned to achieve its best possible response. This superiority is evident across the following key indicators:

— **Output voltage :** ADRC exhibited high accuracy and fast tracking of the reference voltage with minimal overshoot and quicker settling time. In contrast, PID showed slower responses and noticeable oscillations, especially after changes occurred.
— **Control signal :** The control signal generated by ADRC was smoother and more stable, consistently remaining within the operational limits without approaching saturation. PID, however, produced more oscillatory and aggressive control actions following system disturbances.
— **Tracking error :** The tracking error under ADRC remained significantly lower and shorter in duration, indicating more precise control. PID, on the other hand, exhibited larger and more persistent errors.
— **Inductor current :** ADRC produced a higher current immediately after disturbances, reflecting a faster dynamic response. In subsequent intervals, PID showed larger current peaks, likely due to insufficient damping or delayed overcompensation.

Overall, the results confirm that ADRC offers faster response, higher control precision, and better robustness under dynamic conditions involving reference changes, input voltage disturbances, and load variations making it a more reliable solution for controlling the push-pull converter in practical applications.

4.9 Conclusion

This chapter presented a detailed simulation model of the push-pull converter using transfer function representations in Simulink, integrating both PID and ADRC controllers for performance comparison. Three test scenarios were implemented reference voltage variation, input voltage disturbances, and load resistance changes to assess the system's dynamic response under different operating conditions.

The simulation results clearly demonstrated the superiority of the ADRC controller across all scenarios. ADRC achieved faster responses, lower tracking errors, and more stable control signals compared to the optimized PID. The control input generated by ADRC remained smooth and within operational bounds throughout. These findings confirm ADRC's effectiveness and robustness in power conversion applications that demand precise and reliable control.

General Conclusion

This thesis addresses the modeling, control, and simulation of a DC-DC Push-Pull Converter using an Active Disturbance Rejection Control (ADRC) strategy. The converter topology, widely used in medium- and high-power applications requiring electrical isolation, was first analyzed to understand its operation, advantages, and the challenges it presents in dynamic regulation. The average mathematical model of the push-pull converter was derived based on state-space representation, providing a foundation for advanced control design.

In response to the inherent nonlinearity, disturbances, and parameter uncertainties typical in power converters, an ADRC controller was developed. This approach employs an Extended State Observer (ESO) to estimate and compensate for total disturbances in real-time, enhancing system robustness without requiring an exact model of the plant. The control law was formulated using state feedback and the observer output, resulting in a structure that effectively decouples the control task from unknown dynamics.

To validate the effectiveness of the proposed controller, a simulation model was built in MATLAB/Simulink using Transfer Function blocks derived from the averaged system. Three test scenarios were considered to evaluate the controller's performance: variation of the reference output voltage, input voltage disturbance, and load resistance change. Each case compared ADRC with conventional PID control under identical conditions. The results demonstrated the superior transient response, disturbance rejection, and current regulation achieved by ADRC, especially in terms of settling time, overshoot, and control signal smoothness.

Overall, the study confirms the potential of ADRC as a reliable and adaptable control solution for push-pull converters. Its model-independent nature and ability to reject disturbances in real-time make it an attractive choice for advanced power electronic applications, where precision, robustness, and efficiency are paramount.

Appendix

The following figure shows the real images of the Push-Pull Converter used in this study and the digital control board used to generate the switching signal.

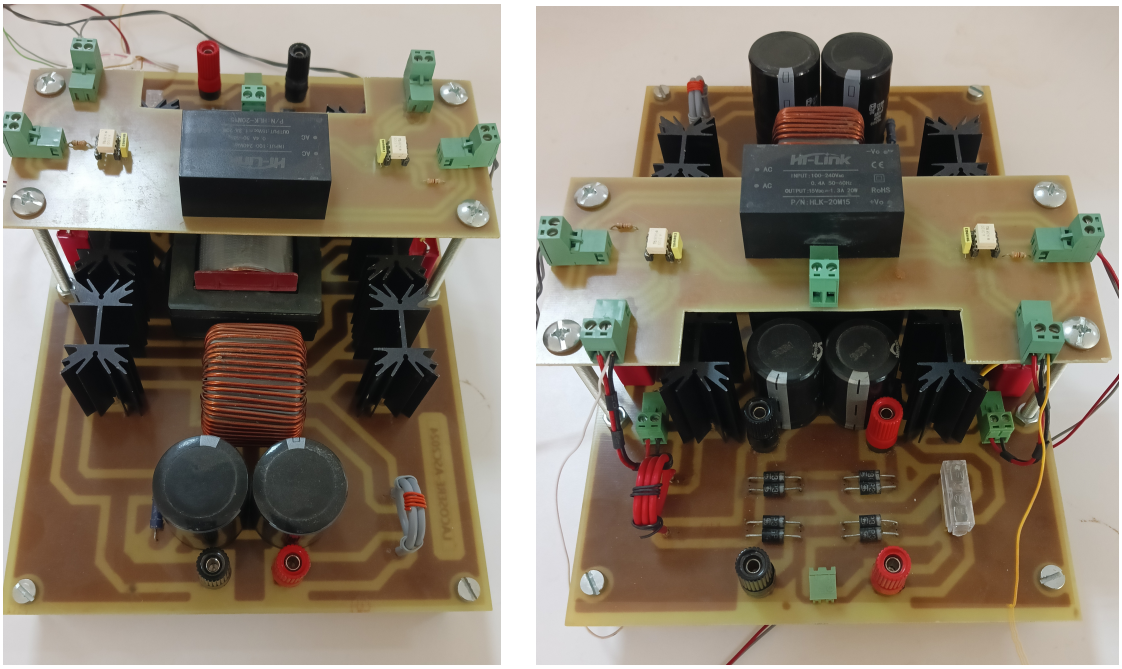

Figure 4.17: Front View of the Push-Pull Converter.

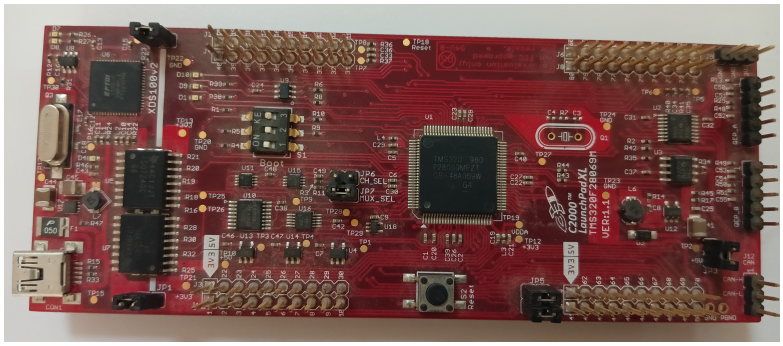

Figure 4.18: Top View of the digital Control board.

Bibliography

[1] Raksha Adappa and K Suryanarayana. Modeling and analysis of 1.2 kw, 36–375 v, push–pull converter. In *Advances in Renewable Energy and Electric Vehicles: Select Proceedings of AREEV 2020*, pages 291–305. Springer, 2022.

[2] Mohammed Benmiloud, Aboubakeur Hadjaissa, Nabil Abouchabana, Khaled Ameur, Attalah Benalia, and Abdelhamid Rabhi. Design and control of pv emulator based on dc-dc push-pull converter. In *2023 International Conference on Electrical Engineering and Advanced Technology (ICEEAT)*, volume 1, pages 1–6, 2023.

[3] Pedram Ghalebani, Vahid Teymoori, and Fredrick Mukundi Mwaniki. Digital peak current mode control of isolated current-fed push-pull dc-dc converter with slope compensation. *International Journal of Circuit Theory and Applications*, 50:779 – 793, 2021.

[4] S.A. Gorji, M. Ektesabi, and J. Zheng. Isolated switched-boost push–pull dc–dc converter for step-up applications. *Electronics Letters*, 53(3):177–179, 2017.

[5] Baoling Guo, Seddik Bacha, and Mazen Alamir. A review on adrc based pmsm control designs. In *IECON 2017-43rd annual conference of the IEEE industrial electronics society*, pages 1747–1753. IEEE, 2017.

[6] Aboubakeur Hadjaissa, Mohammed Benmiloud, Khaled Ameur, Halima Bouchenak, and Maria Dimeh. Advanced photovoltaic emulator with ann-based modeling using a dc-dc push-pull converter and lqr control with current observer. *IRANIAN JOURNAL OF ELECTRICAL AND ELECTRONIC ENGINEERING*, 20(4), 2024.

[7] Albertus Hendra, Fanniesha Hamada, and Feri Yusivar. Voltage control in push-pull dc-dc converter using state space averaging pid with soft-start for electric vehicle auxiliary system. In *2019 6th International Conference on Instrumentation, Control, and Automation (ICA)*, pages 188–193, 2019.

[8] Gernot Herbst. A simulative study on active disturbance rejection control (adrc) as a control tool for practitioners. *ArXiv*, abs/1908.04596, 2013.

[9] Gernot Herbst and Rafal Madonski. *Active Disturbance Rejection Control: From Principles to Practice*. Springer Nature, 2025.

[10] Shudan Jin, Shengrong Zhuo, and Yigeng Huangfu. Design of adrc based on improved eso for enhanced robustness of bidirectional dc/dc converters in dc microgrid. In *IECON 2023-49th Annual Conference of the IEEE Industrial Electronics Society*, pages 1–6. IEEE, 2023.

[11] Zhongjian Kang and Yuntong Li. Active disturbance rejection control of full-bridge dc–dc converter for a pulse power supply with controllable charging time. *Electronics*, 12(24):5018, 2023.

[12] Jong-Won Lim, Changkyu Bai, Tsegaab Alemayehu Wagaye, Ji-Ho Choi, and Minsung Kim. Highly reliable push–pull resonant dc/dc converter for medium-power applications. *IEEE Transactions on Industrial Electronics*, 70(2):1342–1355, 2023.

[13] Rafal Madonski, Krzysztof Łakomy, and Jun Yang. Simplifying adrc design with error-based framework: case study of a dc–dc buck power converter. *Control Theory and Technology*, 19:94 – 112, 2021.

[14] Hebertt Sira-Ramírez, Alberto Luviano-Juárez, Mario Ramírez-Neria, and Eric William Zurita-Bustamante. *Active disturbance rejection control of dynamic systems: a flatness based approach*. Butterworth-Heinemann, 2017.

[15] C.L. Trujillo, D. Velasco, E. Figueres, G. Garcerá, and R. Ortega. Modeling and control of a push–pull converter for photovoltaic microinverters operating in island mode. *Applied Energy*, 88(8):2824–2834, 2011.

[16] Hilmi Zenk. Comparison of the performance of photovoltaic power generation-consumption system with push-pull converter under the effect of five different types of controllers. *International Journal of Photoenergy*, 2019(1):3810970, 2019.

[17] Krzysztof Łakomy, Rafal Madonski, Bin Dai, Jun Yang, Piotr Kicki, Maral Ansari, and Shihua Li. Active disturbance rejection control design with suppression of sensor noise effects in application to dc–dc buck power converter. *IEEE Transactions on Industrial Electronics*, 69:816–824, 2021.